Journal of Building Engineering 70 (2023) 106340

Contents lists available at ScienceDirect

Journal of Building Engineering

journal homepage: www.elsevier.com/locate/jobe

The stiffness of beam-to-RHS joints with welded studs

Ismael García *, Miguel A. Serrano, Carlos López-Colina, Fernando L. Gayarre

University of Oviedo, Dep. Construction and Manufacturing Engineering, Campus Gijón, 33203, Spain

ARTICLE INFO

Keywords:
Tubular structures
Welded studs
Bolted connections
Joint characterization
Demountable construction
Component method

ABSTRACT

The design of demountable bolted beam-to-column joints between structural open profiles as beams and structural hollow-section as columns (IR joints) is not easy. This is because placing bolts in the inner part of the hollow-section column is sometimes difficult or impossible due to their inaccessible interior. The research community has proposed some new types of I-beam to RHS column joints. Blind bolted angle connections, channel/angle connections or angle connections with welded studs are some examples. IR beam-to-column joints with welded studs is great of interest due to their easy on-site execution and their capacity to be disassembled, allowing the members of the joints to be removed, reused, and recycled, contributing to a more sustainable construction. Two analytical models for the stiffness estimation based on the component method are presented in this article. The analytical equations are tested against finite element simulations which has been previously validated through a comparison with the results from full-scale experimental tests. The experimental results were obtained in a vast campaign including single-side or double-side bolted beam-column joints. The results of the forty-nine geometries of beam to column joints analyzed in this paper show that stiffness can be estimated using the proposed analytical models with a reasonable level of accuracy. Finally, a simplified analytical equation to estimate the initial stiffness of the studied joints has been also proposed.

1. Introduction

In steel building construction, I or H open-section profiles have traditionally been used rather than hollow-section profiles due to their lower price per ton. However, hollow-section profiles have advantages in terms of mechanical strength, greater resistance to fire and lower maintenance [1]. Thus, designs using hollow sections can be more efficient than those with open sections in many cases.

When tubular section columns are used, welded joints are usually preferred to bolted joints because they generally imply greater stiffness and resistance [2–4]. However, they have some disadvantages because they require more time and specialization from the operators in the execution task and the joints cannot be easily disassembled. So, the possibilities of reuse or recycle them are notably reduced. Design of bolted joints with structural hollow-sections is not easy because placing bolts in the inner part of hollow-section is sometimes difficult or impossible due to their inaccessible interior. However, the use of bolted joints makes it possible to disassemble the joints, reduces the risks associated with assembly, promotes a greater flexibility and capacity to adapt to new scenarios and, as the members can be disassembled, they can be reused or recycled contributing to a more environmentally responsible building life-cycle [5,6].

In the last years, the use of bolted joints connecting hollow steel columns and I-beam has been studied by some authors. Málaga-

* Corresponding author.
E-mail address: garciaismael@uniovi.es (I. García).

https://doi.org/10.1016/j.jobe.2023.106340
Received 22 December 2022; Received in revised form 10 March 2023; Accepted 18 March 2023
Available online 24 March 2023

Chuquitaype et al. [7,8] proposed the use of blind bolts or "Hollo-bolts" that only requires accessing from one side of the hollow structural section. However, when using concrete-filled tubular steel sections, the joint cannot be disassembled while in non-filled tubular sections a prying tool is necessary to disassemble the joint. Another alternative was proposed by Málaga-Chuquitaype et al. [9] and Liu et al. [10,11] who proposed a kind of connection which requires a channel and an angle cleat as intermediate pieces. In this joint, the channel must be previously welded to the column making the assembling expensive and more complex. An option that makes the joint demountable, when using concrete-filled columns and non requires intermediate pieces, is the use of joints with welded studs. This low-cost technique, which only requires welding threaded studs to the frontal face of the hollow section by using a stud welding gun, was initially proposed in the CIDECT 5AG project by Maquoi [12,13] and later has been studied by Vandegans et al. [14–16], Neves et al. [17] and Serrano et al. [18,19].

When designing and executing structures with these joints, it is necessary to know the mechanical behavior of the joints in terms of stiffness and strength for the reliability of joints and connected members. Eurocode 3.(1.8) [20] includes procedures to estimate the stiffness and resistance of different types of joints using the component method as a way to classify the joint by its rotational stiffness (pinned, semi-rigid and rigid) and by its moment resistance (pinned, partial-strength and full-strength). To apply the component method, firstly, the components which have more influence on the mechanical behavior of the joints (active components) must be identified. Then, the active components are isolated, and their behaviors are simplified by considering them as uniaxial springs with linear stiffnesses calculated through simple equations. Finally, the isolated components are assembled in a mechanical model of the joint, allowing the mechanical behavior of the full joint to be calculated, including its rotational stiffness.

Even though the component method is highly useful and adaptable, as it was initially developed for joints involving open-section profiles, joints formed by open-section beams and hollow-section columns are not included in the standardized analytical proposals of application. For this reason, the prediction of the rotational stiffness of these joints should be obtained through finite element simulations or through expensive experimental tests. Nevertheless, if some validated analytical equations for the stiffness and resistance of the specific components of tubular columns were available, the component method could be applied and the procedure for a reliable characterization of these joints would be simplified.

In this work, beam-column demountable joints formed by tubular columns and open-section beams are studied. These joints are bolted and are executed by means of threaded studs welded to the face of the tube and by using top and seat angle cleats. This type of connection, also called flange-cleat joint, include unequal sided angle cleats to connect the beam flanges to the column faces. In this paper, firstly, a set of 49 beam-column joints that can be used in low-rise building structures is designed. Secondly, a parametric finite element model of these joints is developed, validated and the results are compared with those obtained in full-scale tests carried out by the authors in previous works [18]. Then, two analytical models able to describe the mechanical behavior of the joints and based on the component method are proposed. To achieve this aim, the equations for open sections proposed in Eurocode 3 have been adapted when possible, and some new expressions have been proposed when it was not possible. Finally, a simplified equation to obtain the stiffness of the joints is proposed and the range of applicability is discussed.

2. Experimental and numerical studies

Thirteen full-scale hollow-column to I-beam bolted joints with double angle cleat were tested to obtain the actual moment-rotation curve of the joint. From it, the two main representative values of the joint behavior were obtained: rotational stiffness and moment resistance. The experimental moment-rotation curves allowed its comparison with the results from numerical simulations carried out through the finite element method. Once the numerical simulations were validated through the tests, they were used to extend the model to other untested geometries, which allowed obtaining the rotational stiffness of those different geometries. The results obtained through the experimental and numerical moment-rotation curves were finally used to validate the analytical expressions proposed to obtain the stiffness and resistance of the whole joint. They are mainly the result of assemble the main components that could be identified and characterized through simplified equations.

Fig. 1. Type of beam-column joint tested. (a) Beam connection to one side of the column (SMS); (b) Connection with beam on both sides of the column (DMS).

2.1. Experimental program

For the experimental evaluation of the stiffness of the beam-to-column joints with welded studs, two different types of joints were considered: a) a beam connected to one side of the column (denoted as SMS here) and b) beams connected to both sides of the column (coded as DMS). An example of each type can be seen in Fig. 1. The detailed experimental study was published by the authors in a previous article [18].

The SMS-joints are made up of a square (SHS) or rectangular (RHS) hollow section column with a nominal length of 900 mm, an HEB 200 or IPE 300 beam with a nominal length of 840 mm and angle cleats with unequal sides type L 120 × 80 × 10 connecting the flanges of the beam to the frontal face of the tube. In this type of joints, metric thread bolts, of 16 mm in diameter and quality 8.8 were used to connect one side of the angles to the flanges of the beam. The connection of the other side of angles to the frontal face of the tube was done by means of welded threaded studs with reduced diameter in the non-threaded area, with a metric thread M16, quality K800 and 40 mm length. The different beam-column joint configurations at one side can be seen in Table 1 (specimens SMS), where the relationship between the beam width and the column width (denoted as parameter β) is shown in the last column.

The DMS-joints are made up of a square (SHS) or rectangular (RHS) hollow section column with a nominal length of 900 mm, two HEB 200 or IPE 300 beams with a nominal length of 470 mm and four angles with unequal sides L 120 × 80 × 10. These sections allowed the study of joints with ratios between beam width and column width of $\beta = 1$ and $\beta = 0.75$. To connect the angle cleats to the beams, 16 mm 8.8 bolts were used, while to connect the other side of the angle cleat to the column, welded studs with a reduced diameter in the non-threaded area were used. The studs were 16 mm and 4.8 grade and their length were 35 mm. The different beam-column joint configurations with beams on both sides of the column can be seen in Table 1.

Table 2 shows the dimensions of the studs used according to the geometric parameters showed in Fig. 2. The geometry of the angle cleats with the positions of the holes can be seen in Fig. 3. The distances of the holes to the edge were selected according to the minimum and maximum distances established by Eurocode 3.(1.8) [20]. The bolts were prestressed with a tightening torque of 190 Nm applied in two steps. Thus, a torque of 150 Nm was initially applied, while in a second step the bolts were prestressed up to 190 Nm.

2.2. Numerical model of the joints

The numerical simulations of the beam-column joints (Fig. 1) were carried out by means of the Finite Element software ANSYS 18.1. Parametric models that allow an easy adaptation to different dimensions of the joints were developed considering geometrical and material non-linearities. Different levels of detail were tested in the simulations in order to finally select the simplest one that shows enough accuracy for obtaining the initial rotational stiffness in a parametric study.

2.2.1. Simulation with solid elements

A complete finite element simulation with solid elements including bolts, nuts, studs and all the corresponding contacts was performed to compare its results with both the experimental ones and those from a simpler FE model. Three solid 186 elements were considered through all wall thicknesses and geometric and material non-linearities were considered. A complete non-linear stress-strain curve was taken for the material properties of the cold-formed hollow sections. The experimental results of yield limit and ultimate strength from coupons extracted of different sections were considered for this material and the complete curve was created by following the Ramberg & Osgood [21] nonlinear model until the yield limit (1). After this point, the Mirambell & Real [22] proposal (2) was used.

$$\varepsilon = \frac{\sigma}{E} + 0.002 \cdot \left(\frac{\sigma}{f_y}\right)^n \quad \text{if } \sigma \leq f_y \tag{1}$$

$$\varepsilon = \frac{\sigma - f_y}{E_{0.2}} + \left(\varepsilon_u - \varepsilon_{0.2} - \frac{f_u - f_y}{E_{0.2}}\right) \cdot \left(\frac{\sigma - f_y}{f_u - f_y}\right)^m + \varepsilon_{0.2} \quad \text{if } \sigma > f_y \tag{2}$$

Where f_y is the yield limit (0.2% proof stress) and the slope at 0.2% proof stress is $E_{0.2}$ (3) and the strain at that point is $\varepsilon_{0.2}$ (4).

Table 1
Set-up of the beam-column joints tested with beam on one side (SMS) and beam on both sides (DMS).

Specimen	Column	Beam	Angle cleat	Bolts	Studs	β [b_b/b_0]
SMS1	SHS 200.6	HEB 200	L120 × 80 × 10	8 × M16 8.8	4 M16 × 40 K800	1
SMS2	SHS 200.8	HEB 200	L120 × 80 × 10	8 × M16 8.8	4 M16 × 40 K800	1
SMS3	SHS 200.10	HEB 200	L120 × 80 × 10	8 × M16 8.8	4 M16 × 40 K800	1
SMS4	SHS 200.6	IPE 300	L120 × 80 × 10	8 × M16 8.8	4 M16 × 40 K800	0.75
SMS5	SHS 200.8	IPE 300	L120 × 80 × 10	8 × M16 8.8	4 M16 × 40 K800	0.75
SMS6	SHS 200.10	IPE 300	L120 × 80 × 10	8 × M16 8.8	4 M16 × 40 K800	0.75
SMS7	RHS 200.150.6	IPE 300	L120 × 80 × 10	8 × M16 8.8	4 M16 × 40 K800	1
SMS8	RHS 200.150.8	IPE 300	L120 × 80 × 10	8 × M16 8.8	4 M16 × 40 K800	1
SMS9	RHS 200.150.10	IPE 300	L120 × 80 × 10	8 × M16 8.8	4 M16 × 40 K800	1
DMS1	SHS 200.8	HEB 200	L120 × 80 × 10	16 × M16 8.8	8 M16 × 35 4.8	1
DMS2	SHS 200.6	IPE 300	L120 × 80 × 10	16 × M16 8.8	8 M16 × 35 4.8	0.75
DMS3	SHS 200.8	IPE 300	L120 × 80 × 10	16 × M16 8.8	8 M16 × 35 4.8	0.75
DMS4	RHS 200.150.8	IPE 300	L120 × 80 × 10	16 × M16 8.8	8 M16 × 35 4.8	1

Table 2
Geometric properties of the studs.

d_1	class	l_2 [mm]	d_2 [mm]	d_3 [mm]	y_{min} [mm]	h_1 [mm]	Ceramic ferrule
M16	K800	40	13.2	18	11	6	RF16
M16	4.8	35	13.2	18	11	6	RF16

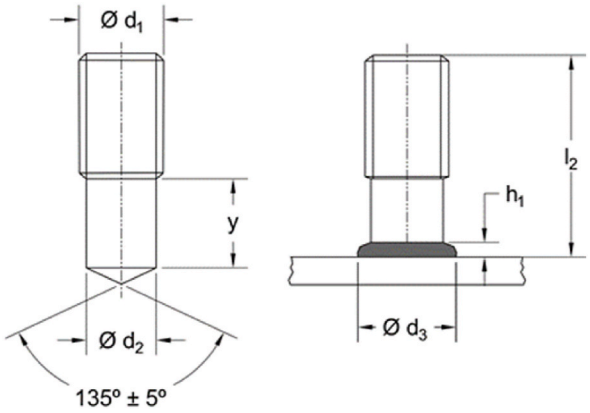

Fig. 2. Geometric parameters of the studs: before welded (left) and once welded (right).

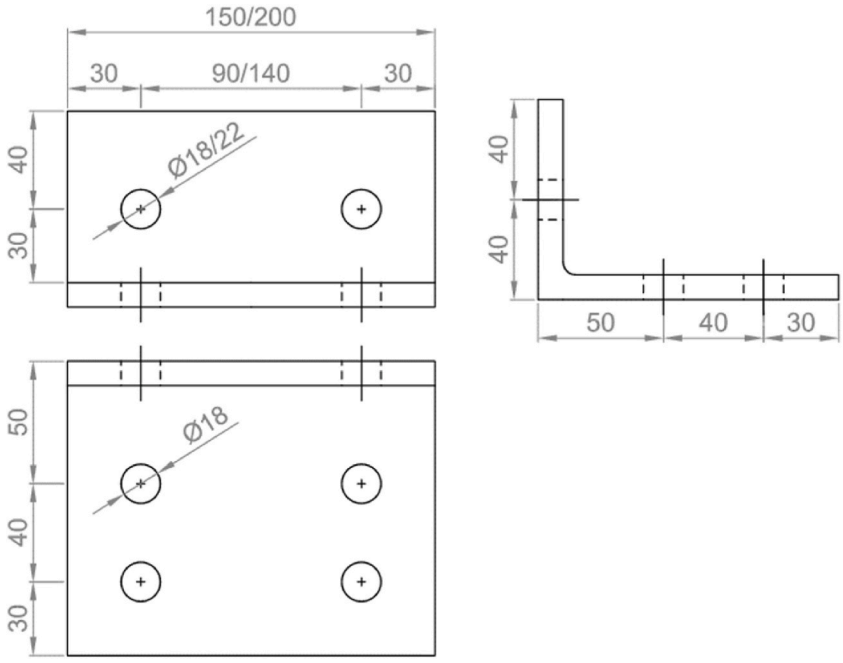

Fig. 3. Geometry of the angle cleats and position of the holes.

$$E_{0.2} = \frac{E}{1 + 0.002 \cdot n \cdot \left(E/f_y\right)} \tag{3}$$

$$\varepsilon_{0.2} = \frac{f_y}{E} + 0.002 \tag{4}$$

The parameters m and n are constants that depend on the material being considered. With the experimental characterization tests the parameters were adjusted to n = 8 and m = 2. The comparison between the stress-strain experimental and the mentioned material model with n = 8 and m = 2 is presented in Fig. 4 for the cold-formed SHS200 × 6 (S275J0H).

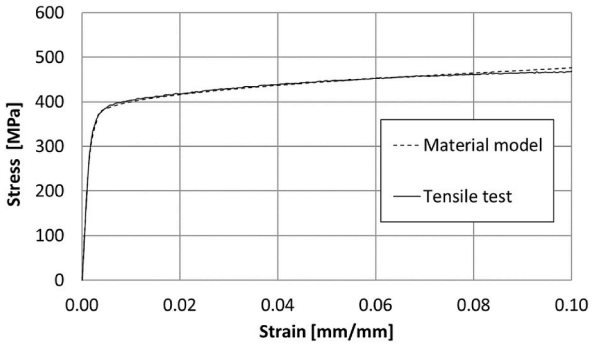

Fig. 4. Comparison between material model and tensile test SHS200 × 6.

The material model was bi-linear for the hot-rolled steel pieces, with a strain-hardening slope $E_{sh} = 0.015$ E, as recommended by Foster et al. [23] when $f_u/f_y > 1.3$.

The mechanical behavior of studs and bolts was simplified as a bi-linear curve with $E_{sh} = 0{,}0001$ E, which is the recommended value in EC3-1.5 [24] when strain hardening is not expected to be significant.

The geometry was meshed adopting an element size of 3 mm in the most critical areas and components: bolts, angle cleats, studs and compression and tension zones in the hollow section (see Fig. 5). In order to save computational time, double symmetry was considered since the numerically simulated tests was the double-side monotonic (DM) for joint DMS3 (Fig. 5a).

2.2.2. *Simulation with shell elements*

In order to develop a simplified model useful for wide parametric studies and practitioners, shell 181 elements were taken for the walls of tubes as well as for the flanges, the web of the connected beams and the angle cleats. These types of elements were calibrated and validated recently for welded I-to-RHS connections in Ref. [25] or for I-to-RHS end-plate bolted connections in Ref. [26] and they were demonstrated to give good results and efficient computation time.

Two simple considerations of bolts and studs were tested in the simulations by considering a bonded contact between the hole edges and the stud perimeter welds and by using preloaded line elements. The first simplification is implicitly neglecting the bolt and stud deformations against the deformation of the other components, but the difference between both methods was not significant when low and medium loads are considered due to the preload that was applied to the fasteners. Therefore, the simplest model can be used in most of cases for obtaining the initial stiffness. When the moment resistance does not depend on the premature fracture of the studs it was necessary to simulate them with preloaded line elements to take into account their deformation and to obtain a good approximation to the experimental moment-rotation curve (see detail in Fig. 5c).

The use of shell elements for the connection studied here is partially supported by the work in Ref. [15], where only the component "frontal face in tension" is modelled. However, a validation of the complete shell model is still necessary since it includes many other sources of uncertainty like the mentioned contacts or the simplified consideration of bolts and studs.

For all pieces, the stress-strain curve was assumed to be bilinear elastic-plastic with a linear strain hardening part that has a slope of $E_{sh} = 0.015$ E = 3090 MPa in the plastic zone of the curve. This is the recommendation by Foster et al. [23] when $f_u/f_y > 1.3$ for hot rolled I sections and when $f_u/f_y > 1.15$ for cold-formed hollow sections. The actual yield limits for tube walls and IPE were considered from the tests results on coupons extracted from the faces of the hollow sections and webs and flanges from the open profiles [18].

Due to the symmetry of loads and geometry, just half of the full joint was considered in the DMS models allowing to save computation time (see Fig. 5c). The model for the validation was created by considering the measured dimensions of the specimens. The DMS tests were simulated introducing a vertical displacement, according to the applied compression load, on top of the column while the double-sided beam-column joints were simply supported at the ends of both beams. The SMS simulations were designed with a vertical imposed displacement on the beam end as in the experimental tests.

The bending moment was calculated in the connection plane and was registered to be plotted versus the corresponding rotation of the beam measured 60 mm away (point denoted as 'A' in Fig. 5b).

The mesh size was calibrated prior to the experimental validation by considering quadrilateral shell elements of about 5, 7.5 and 10-mm sizes in the columns and angles. Since the beam is expected to have much less influence on the joint behavior, the main size of its elements was taken as the double of the mentioned values. As an example, the result of this calibration for the DMS4 specimen is shown in Fig. 6. It shows no differences between the three moment-rotation curves at low deformation levels and even at higher rotations, the differences are almost negligible between the finest and medium mesh if we consider that the rotation for a transverse deformation of the column of $3\%b_0$ [2] that determines the failure is at about 0.026 rad. This transverse deformation was obtained in the studs under tension of the FE models (see Fig. 5b).The results leaded to take a mesh of 7.5 mm for the column and the angles and a mesh size of 15 mm for the beam.

2.3. *Comparison solid elements vs. simplified simulation*

Fig. 7 shows the comparison between the results from the complete FE simulation with solid elements and the simplified shell model for the DMS2 test. The test result is also reproduced in the graph. The numerical curves show good agreement between them and

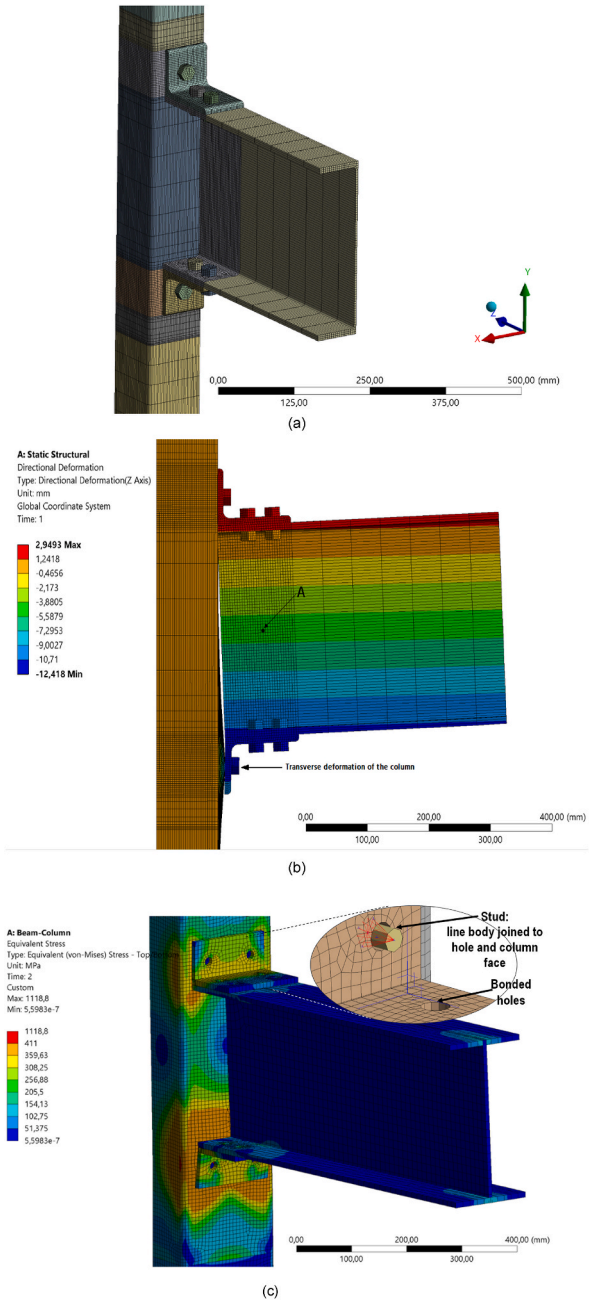

Fig. 5. DMS3 simulation: one quarter model mesh (a) and Horizontal displacement (b) with solid elements and Von misses stress of the half model with shell elements (c).

between them and experimental results. In order to fairly assess the results, it should be taken into account that neither the complete simulation nor the simplified one are able to predict the fracture. As it was said by Van der Vegte et al. [27], common FE models cannot simulate cracking and fracture and some other more sophisticated models such as critical strain or damage criterion are required.

The squared points marked in the FEM curves show the instant when a transverse deformation of $3\%b_0$ (6 mm for the SHS200 × 6) is reached in the simulations. Although in the simplified shell simulation the moment-rotation curve shows more divergence beyond that point, the stiffness overestimation by the solid model, together with the good agreement of the simplified FE model before that point and its very low computation time led to consider it as suitable for further parametric studies.

According to these results, the work continues with the complete validation of the simplified FE simulation with experimental results since it has been demonstrated that it can provide enough accurate response curves in the part where initial stiffness is measured, with a very limited computation time and number of elements.

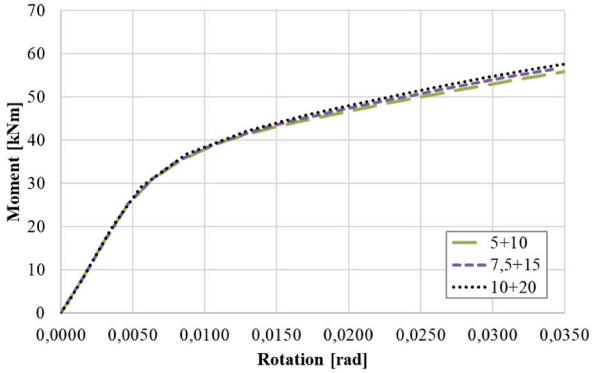

Fig. 6. Mesh size calibration with DMS4 FE model.

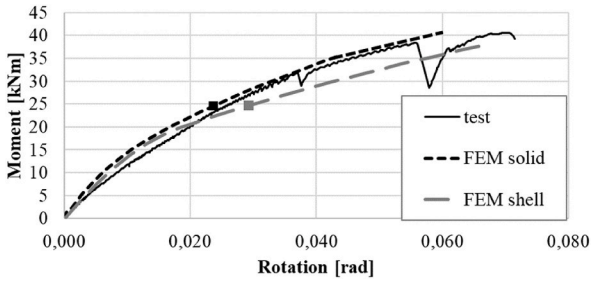

Fig. 7. Comparison solid vs. simplified simulation (DMS2).

2.4. Experimental validation of the simplified simulation

Table 3 presents a comparison of the results obtained for the initial rotational stiffness S_{ini} from the experimental tests and their corresponding FE simulation for joints with a beam section HEB200 and a width ratio $\beta = 1$. The initial stiffness was taken as the slope of the linear regression for the data points prior to a rotation angel of 3 mrad (0.003 rad). Table 4 presents the above-mentioned comparison in case of beam sections IPE300 and considering separately joints with width ratios $\beta = 0.75$ and $\beta = 1.0$. Good agreement was obtained in most cases with a mean value of deviations lower than 5%. It should be considered that there are inherent difficulties on the initial rotational stiffness measurement due to the variability of the connecting components fit and the nonlinear behavior of the joint since the beginning of the loading process. However, the proposed simplified finite element model provides enough accuracy for the stiffness assessment and can be used in further extensions of the study.

The comparison between the simplified FE model and experimental tests shows good agreement for low rotations. Therefore, it can be an efficient method for the simulation of the initial stiffness. Some tests (mainly the DMS set) show some differences at higher loads when some downward peaks caused by premature cracking in the studs or in their welding area appear, and they cannot be simulated by the model. However, after them, finite element simulations and experimental results tend to converge.

Figs. 8–11 present the experimental moment-rotation curves and their FE simulation for comparison for the batches of joints DMS, SMS1-SMS3, SMS4-SMS6 and SMS7-SMS9. Since DMS experimental tests presented a much more ductile behavior on their 4.8 studs after the first cracks, those were simulated until high rotations. The failure of the K800 studs used in SMS tests gave experimental curves with lower rotation capacity. In both cases the simulation cannot predict neither the cracks nor the fragile failure of the studs or their welds. Therefore, an analytically predicted fracture of the studs considering the failure mechanisms of the equivalent T-stub [9], is presented in the FEM curves as a squared point. The calculations to obtain these resistance values have been carried out assuming the actual material properties provided by the manufacturer [28] in the case of DMS simulations and with the experimental material properties obtained from the results of section 2.2.1 in case of the SMS models. In addition, some cross points have been placed marking the values in which the analytical front-face failure (according to Grotmann & Sedlaceck [29]) predicted smaller values than the resistance of the bolts.

A quite good general agreement can be observed not only in terms of initial rotational stiffness as above commented but also for the

Table 3
S_{ini} [kNm/rad] of joints with an HEB200 as a beam.

Width ratio $\beta = 1.0$	DMS1 t = 8 mm	SMS1 t = 6 mm	SMS2 t = 8 mm	SMS3 t = 10 mm
Test	2744	1973	2801	3671
FEA	2529	2086	2920	3591

Table 4
S_{ini} [kNm/rad] of joints with an IPE300 as a beam.

Width ratio β = 0.75	DMS2 t = 6 mm	DMS3 t = 8 mm	SMS4 t = 6 mm	SMS5 t = 8 mm	SMS6 t = 10 mm
Test	1384	2882	2050	3795	4945
FEA	1472	2643	1790	3421	5476
Width ratio β = 1.0	DMS4 t = 8 mm	SMS7 t = 6 mm	SMS8 t = 8 mm	SMS9 t = 10 mm	
Test	5924	3828	5886	9303	
FEA	5524	3878	5786	8890	

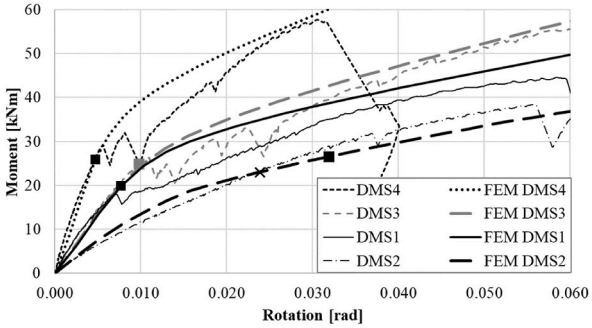

Fig. 8. Moment-rotation curves for DMS tests and FEM.

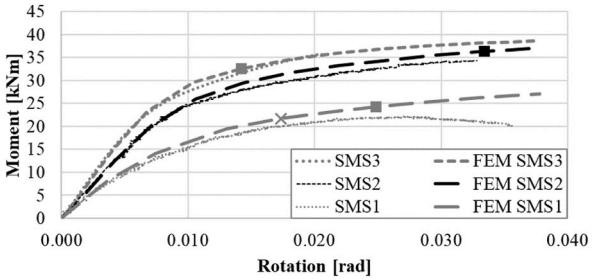

Fig. 9. Moment-rotation curves for SMS1 to SMS3 tests and FEM.

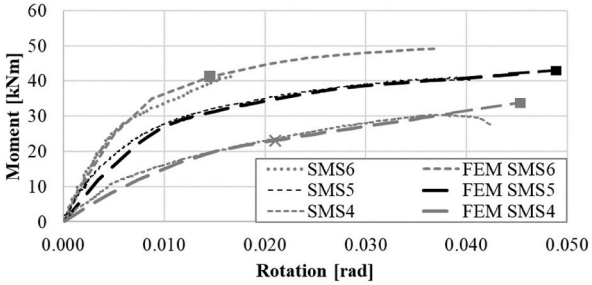

Fig. 10. Moment-rotation curves for SMS4 to SMS6 tests and FEM.

value of joint resistance. It is worth noting that, since the proposed models cannot simulate a fragile fracture, they present ductile behavior after yielding and until the predicted failure of studs is reached.

The combination of FE simulation and the approximate calculation of stud resistances gives good agreement in both terms of stiffness and resistance if we consider the first crack for this (see Fig. 8).

2.5. Extension of the simplified simulation

Once the FE model was validated, it was extended to another 36 different geometries of joints in order to study the stiffness of several beam-column joints that are likely to be used in low-rise and medium-rise residential buildings. All the joints considered in the

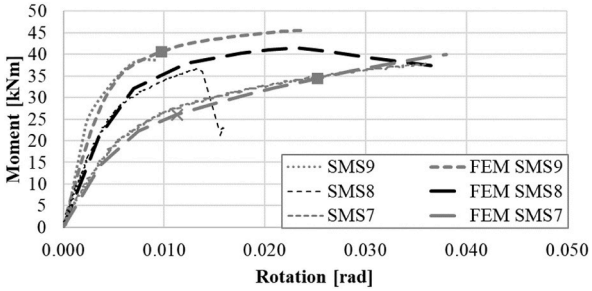

Fig. 11. Moment-rotation curves for SMS7 to SMS9 tests and FEM.

study were joints connecting IPE-section for beams and SHS hollow sections for columns, joined by two types of unequal angle cleats: L120 × 80 × 10 and L120 × 80 × 12. 20 mm welded studs with reduced diameter and 16 mm bolts were used to connect the angle cleats sides to the column and to the beam, respectively. The geometries of the joints that were simulated numerically can be seen in Table 5.

All the joints were designed using angle cleats with the same length as the width of the beams, like in the experimental campaign. The dimensions of the holes and the distances to the edges were the same as those used in the specimens tested experimentally (Fig. 3). For the material properties, the nominal yield strength of S275 steel was used for the beams and columns, and the nominal properties of the K800 stud (E = 210 GPa, f_y = 640 MPa) were used for the studs. The obtained initial rotational stiffnesses for the joints simulated numerically can be seen in Table 5. The joints were classified according to the stiffness classification proposed in Eurocode 3.1.8 [20]. In the classification, typical spans of 30 or 20 times the depth of the HEB or IPE beams were taken. Fig. 12 shows the stiffness classification of the beam-column joints together with the rigid ($S_{j.ini} = 8EI_b/L_b$) and pinned limits ($S_{j.ini} = 0.5\,EI_b/L_b$). From this figure it can be inferred that all the tested beam-column joints and the FEM extended specimens behave as semi-rigid in non-sway frames, with the only exception of DMS2 that is just in the lower limit.

3. Analytical modelling of the joint stiffness

In general, any typical connection configuration can be idealized as an assemblage of uniaxial springs following the component-based method [20,30]. This section evaluates two analytical models based on the component method for the estimation of the rotational stiffness of the proposed joints. Model 1 is a close adaptation of the EC3-1-8 model for open-sections, but it slightly modifies some of the existing component equations or the parameters introduced in them, to be applied to rectangular hollow columns. Model 2 combines some of the equations proposed in EC3 and proposes new ones for the estimation of the stiffness of key components of the RHS column. The two models are then compared in the subsequent section to evaluate the concordance between the rotational stiffness obtained through the analytical models and the experimental and numerical stiffness.

3.1. Spring model 1

Model 1 is a direct adaptation of the EC3-1-8 model for open-sections and takes into account the basic components: lateral faces

Table 5
Geometry and rotational stiffnesses $S_{j,NUM}$ of the joints numerically simulated.

Joint	Beam IPE	Column SHS	Column thickness t_0 [mm]	t_l = 10 mm	t_l = 12 mm
				$S_{j,NUM}$ [kNm/rad]	$S_{j,NUM}$ [kNm/rad]
FEBC01	240	120	6	2587	3630
FEBC02	240	120	8	3358	5040
FEBC03	240	120	10	4103	6480
FEBC04	270	140	6	3247	4470
FEBC05	270	140	8	4504	6750
FEBC06	270	140	10	5237	8030
FEBC07	300	160	6	3990	5340
FEBC08	300	160	8	5594	8220
FEBC09	300	160	10	6555	9750
FEBC10	330	160	6	4982	6660
FEBC11	330	160	8	6508	9310
FEBC12	330	160	10	8043	11,900
FEBC13	360	175	6	5798	7650
FEBC14	360	175	8	8222	11,700
FEBC15	360	175	10	9540	13,900
FEBC16	400	180	6	7284	9430
FEBC17	400	180	8	9618	13,400
FEBC18	400	180	10	11,930	17,100

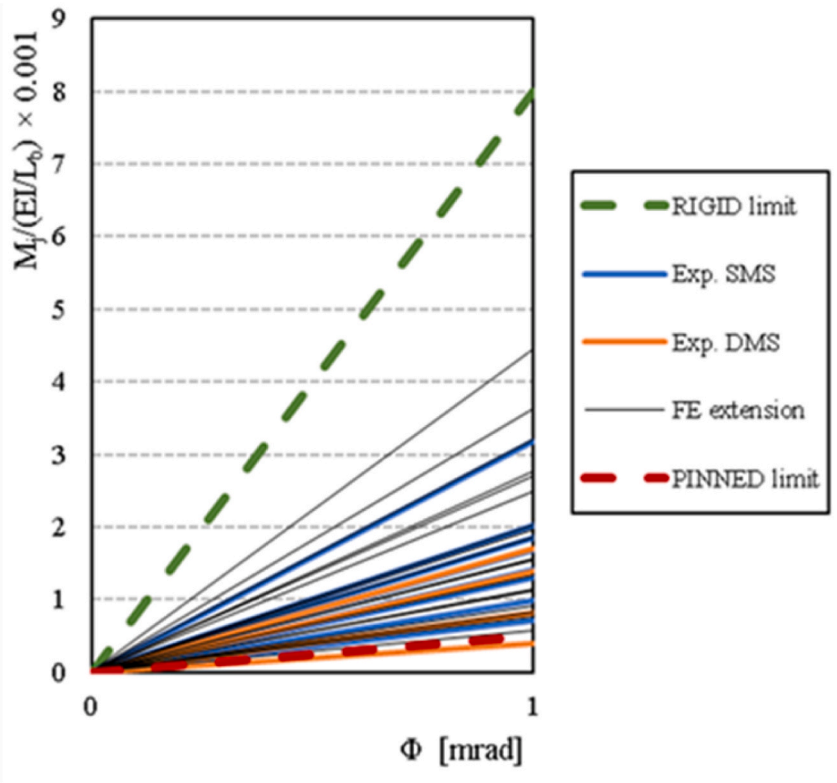

Fig. 12. Stiffness classification of the beam-column joints.

under shear (k_1), lateral faces under compression (k_2), lateral faces in tension (k_3), frontal face in bending (k_4), angle cleats in bending (k_6) and studs in tension (k_{10}). The spring model adopted for the proposed model 1 is presented in Fig. 13, while the joint's geometric parameters, the level arm of the joint (z) and the basic components are identified in Fig. 14. The expressions to determine the stiffness coefficients for basic components have been adapted from the EC3-1-8, section 6.3.2.

3.1.1. Component lateral faces under shear

The stiffness coefficient of the lateral face under shear k_1 has been estimated according to the following equation, proposed in EC3 for the column web under shear when conventional open profiles are used:

$$k_1 = \frac{0.38 \bullet A_v}{\beta_T \bullet z} \tag{5}$$

Where A_V is the shear area of the column. In case of rectangular hollow sections with a load parallel to the depth h_0, A_V can be calculated according to equation (6), where A_T is the cross-sectional area, h_0 and b_0 are respectively the depth and width of the tube, and β_T is a transformation parameter obtained from Eurocode 3.1.8. This parameter varies depending upon loading conditions so, when the column has moments applied to one side of the joint it can be approximated by 1 while if moments are equal and applied to both sides, the parameter β_T is equal to 0. z is the lever arm defined according to Eurocode 3.1.8 for a joint with angle cleats (see Fig. 14).

$$A_v = \frac{A_T \bullet h_0}{b_0 + h_0} \tag{6}$$

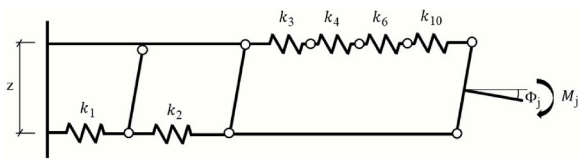

Fig. 13. Simplified spring model of the joint adopted in the proposed model 1.

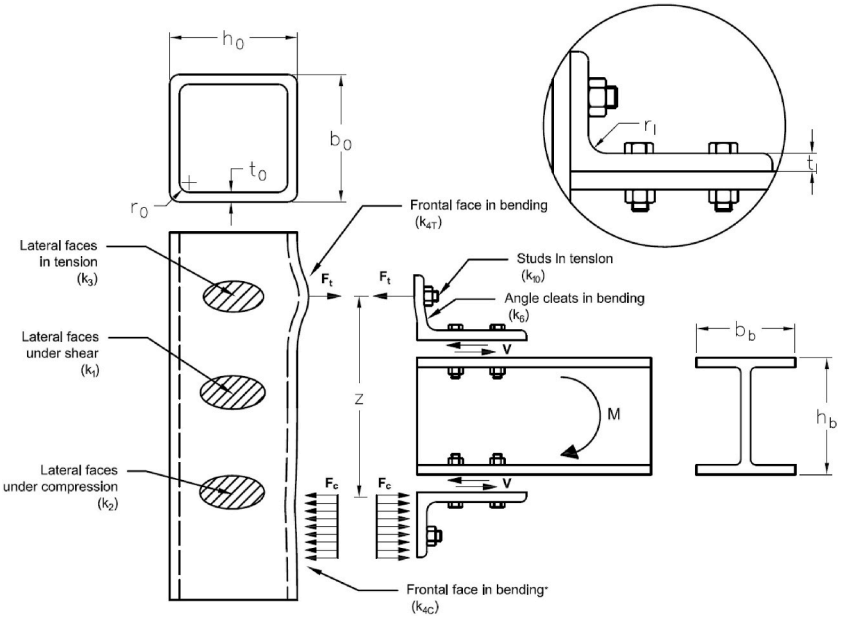

Fig. 14. Sketch of a deformed single-sided joint. Definition of the joint's geometric parameters and lever arm (z). Identification of the main components of the joint (k_i). The basic component identified with '*' is only included in model 2. Notation: M, bending moment; Ft, tensile force; Fc, compression force; V, shear force.

3.1.2. Component lateral faces under compression

The stiffness coefficient of the lateral face under compression k_2 can be determined with equation (7), which is used for the column web under compression in the European code:

$$k_2 = \frac{0.7 \bullet b_{eff} \bullet t_0}{d_c} \tag{7}$$

Where b_{eff} is the effective width of the lateral faces of the column under compression, which, adapting it to RHS, could be calculated using equation (8), in which t_l is the thickness of the angle cleat, r_l is the radius of the angle cleat, t_0 is the thickness of the column, r_0 is the radius of the column and d_c is the width of the tube minus 3 times its thickness.

$$b_{eff} = 2t_l + 0.6r_l + 5 \bullet (t_0 + r_0) \tag{8}$$

3.1.3. Component lateral faces in tension

The coefficient of stiffness of the lateral face in tension k_3 has been obtained according to equation (9), based on the one for the column web under tension in Eurocode.

$$k_3 = \frac{0.7 \bullet \ell_{eff} \bullet t_0}{d_c} \tag{9}$$

Where ℓ_{eff} is the effective width of the lateral faces of the column in tension, which can be calculated according to proposed equation (10), where m is the distance between the stud and the beginning of the radius of curvature of the column, e is the distance from the axis of the stud to the center of the column face, t_0 is the thickness of the column and d_c is the width of the tube minus 3 times its thickness.

$$\ell_{eff} = min(2\pi m, 4m + 1, 25e) \tag{10}$$

3.1.4. Component frontal face in bending

The stiffness coefficient of the frontal face of the column in bending k_4 has been determined by adaption of the equation proposed in EC3 for open sections (11).

$$k_4 = \frac{0.9 \bullet \ell_{eff} \bullet t_0^3}{m^3} \tag{11}$$

where l_{eff} is the effective width of the column (equation (10), t_0 is the thickness of the column and m is the distance between the stud and the beginning of the radius of curvature of the column. This component has been considered once in the assembly (see Fig. 14), referred to the front face in bending of the tension area, being coherent with the proposal of EC3-1.8 for the column flange in double (top and seat) cleat angle connections.

3.1.5. Component angle cleat in bending

The stiffness coefficient of the angle cleats in bending k_6 can be evaluated by (12), by means of the equivalent T-stub procedure suggested in EC3, taking l_{eff} equal to 0.5 times the length of the angle cleat, t_l is the thickness of the angle cleat, and m is the distance between the axis of the stud in tension and the beginning of the radius of curvature of the angle cleat.

$$k_6 = \frac{0.9 \bullet l_{eff} \bullet t_l^3}{m^3} \tag{12}$$

3.1.6. Component studs in tension

The stiffness coefficient of the studs in tension k_{10} has been estimated in concordance with equation (13), used in EC3 for bolts in tension, where A_s is the reduced area of the stud, and L_s is the length of the stud subjected to tension, taken as the thickness of the angle plus the washer and half the height of the nut.

$$k_{10} = \frac{1.6 \bullet A_s}{L_s} \tag{13}$$

3.1.7. Assembling the uniaxial springs

Taking into account the aforementioned stiffness coefficients, the initial stiffness of the full joint $S_{j,M1}$ calculated according to the proposed model 1, can be obtained according to equation (14) of assembly of the components.

$$S_{j,M1} = \frac{E \bullet z^2}{\frac{1}{k_1} + \frac{1}{k_2} + \frac{1}{k_3} + \frac{1}{k_4} + \frac{1}{k_6} + \frac{1}{k_{10}}} \tag{14}$$

3.2. Spring model 2

Model 2 is an improved adaptation of the model proposed by EC3-1-8 for open sections and takes into account the components: lateral face in shear (k_1), lateral faces in compression and tension (k_2 and k_3), frontal face in bending: stud-rows under compression ($k_{4,C}$), frontal face in bending: stud-rows under tension ($k_{4,T}$), angle cleat in bending (k_6) and studs in tension (k_{10}). The spring model adopted for model 2 can be seen in Fig. 15, while the level arm of the joint can be seen in Fig. 14. The main differences with Model 1 are the equations for the lateral faces in tension and compression and for the front faces in bending. In addition, those were considered for both the tension and compression area (see Fig. 15) while in the previous model the effect of the compression component for the front face was neglected.

3.2.1. Component lateral faces under shear

The stiffness of the lateral face under shear k_1 has been determined in the same way as in model 1, according to expression (5).

3.2.2. Components lateral faces under compression and tension

The coefficients of stiffness of the lateral face in compression and tension k_2, k_3 have been obtained by adapting the empirical expression proposed by Aribert et al. [31] for the web of open-section profiles. The original fourth root has been modified, replacing it by an eighth root after an empirical adaptation to joints with RHS profiles, according to studies carried out by some of the authors in previous works on welded beam-column connections (López-Colina et al. [4]; Lozano [32]. The stiffness coefficient of the lateral faces under compression and tension can be calculated with equation (15):

$$k_2 = k_3 = 0.45 \bullet t_0 \bullet \sqrt[8]{\frac{b_0}{h_0}} \tag{15}$$

Where t_0 is the thickness of the column wall, b_0 is the width and h_0 is the depth of the column.

3.2.3. Components frontal face in bending

The coefficients of the frontal face in bending in the compression stud-rows k_{4C} and in the tension stud-rows k_{4T} have been obtained with equation (16), where t_0 is the thickness of the column wall, v is the Poisson's ratio of the material, C_t can be calculated according to equation (17) and 'a' is half the width of the frontal face minus the thickness of the RHS (18).

The value of C_t has been determined according to previous works [32] where a coefficient (β), dependent on the relationship between the width of the column and the width of the tube, is defined. However, in this paper a new β* coefficient is defined, being different in the tension and compression zones. This is because in the stud-rows under tension, the frontal face of the column is tensioned through the studs, but in the stud-rows under compression the load is applied perpendicularly to the column frontal face,

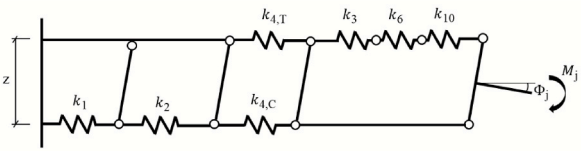

Fig. 15. Simplified spring model of the joint adopted in the proposed model 2.

through the entire surface of the short flange of the angle cleat. Thus, in the case of compression, the new coefficient β* was defined as the ratio between the length of the angle cleat (which in our connections is equal to the width of the beam b_b) and the width of the column (b_0), while for tension it is the ratio between the spacing of the studs and the width of the column (b_0). According to previous works [32], the range of applicability of the equation is limited to values of β* lower than 0.87. For higher values, the effect of the component of stiffness should be neglected.

$$k_{4C} = k_{4T} = \frac{\pi \bullet t_0^3}{12 \bullet (1 - v^2) \bullet C_t \bullet a^2} \tag{16}$$

$$C_t = -0.08 \bullet \beta^* + 0.07 \text{ with } \beta^* < 0.87 \tag{17}$$

$$a = \frac{b_0 - t_0}{2} \tag{18}$$

3.2.4. Components angle cleat in bending and studs in tension

The coefficient of the angle cleat in bending k_6 has been obtained with the expression (12) proposed in Eurocode 3 and which is the same as that used in model 1. Similarly, the estimation of the coefficient of stiffness of the studs in tension k_{10} has been estimated in accordance with expression (13), proposed by Eurocode 3 and is the same as that used in model 1.

3.2.5. Assembling the uniaxial springs

Taking into account the previously mentioned stiffness coefficients, the initial stiffness of the full joint $S_{j,M2}$, calculated according to model 2, can be obtained by equation (19).

$$S_{j,M2} = \frac{E \bullet z^2}{\frac{1}{k_1} + \frac{1}{k_2} + \frac{1}{k_3} + \frac{1}{k_{4C}} + \frac{1}{k_{4T}} + \frac{1}{k_6} + \frac{1}{k_{10}}} \tag{19}$$

4. Discussion

The analytical stiffnesses for the beam-column joints tested experimentally can be seen in Table 6. For an easy comparison, the table shows the initial stiffnesses $S_{j,EXP}$ obtained in the experimental tests carried out on full scale joints, together with the analytical initial stiffness obtained for those joints through the model 1, $S_{j,M1}$ (equation (14)) and the model 2, $S_{j,M2}$ (equation (19)).

All these results from Table 6 are graphically presented together with those from the extension of the finite element model in Figs. 16 and 17. The figures compare the initial stiffnesses obtained in the tests $S_{j,EXP}$, or from the extension of the numerical model of FE with the analytical estimation through models 1, $S_{j,M1}$ (equation (14) in Fig. 16) and model 2, $S_{j,M2}$ (equation (19) in Fig. 17). The solid diagonal line indicates a perfect fit, while the dashed lines show the ±20% interval of error. From the figures it can be inferred that in most cases the model 1 overestimates the actual stiffness of the joint, i.e., the stiffnesses obtained through the model 1 are higher than those obtained experimentally or numerically, while the stiffness obtained through model 2 are in general more precise and with predictions on the safety side.

According to the previous results, an acceptable concordance between the analytical predictions and the experimental results is observed. In the case of model 1, a mean absolute error (MAE) of 23.55% was obtained for the SMS specimens and a MAE of 54.43% for the DMS specimens. The discrepancies are smaller when model 2 is compared with the experimental results, with an average absolute error of 14.65% for the SMS specimens and an average absolute error of 16.56% for the DMS specimens. Similar results were observed when all the available results (numerical and experimental) are compared together with the analytical predictions. In the case of model 1, a MAE of 21.78% was observed when all the stiffness values are included. The discrepancies were again smaller when the results obtained through model 2 were compared, obtaining a mean absolute error (MAE) of 13.26% for the set of all the specimens. Finally, it is observed that the SMS9 specimen does not fit with the trend of the rest of specimens. Since its stiffness is well above the stiffness obtained experimentally for the same joint geometry but with a tube thickness of 8 mm (SMS8 specimen), it is understood that this

Table 6
Initial stiffness obtained in the test $S_{j,\ EXP}$ and initial stiffness obtained through the model 1, $S_{j,M1}$ and the model 2, $S_{j,M2}$.

Specimen	$S_{j,EXP}$ [kNm/rad]	$S_{j,M1}$ [kNm/rad]	$S_{j,M2}$ [kNm/rad]
SMS1	1973	2973	1935
SMS2	2801	3589	2708
SMS3	3671	3834	3212
SMS4	2050	2824	1941
SMS5	3795	4387	3203
SMS6	4945	5360	4220
SMS7	3828	4687	3424
SMS8	5886	5503	4545
SMS9	9303	5773	5104
DMS1	2744	3897	2892
DMS2	1384	2963	2003
DMS3	2882	4637	3322
DMS4	5924	5969	4851

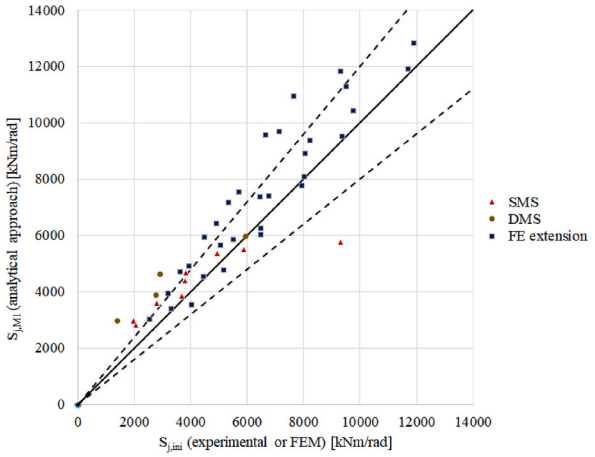

Fig. 16. Assessment of beam to column stiffness analytical approach (model 1).

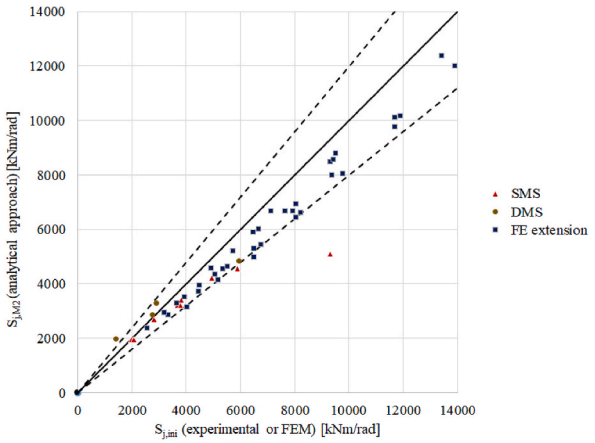

Fig. 17. Assessment of beam to column stiffness analytical approach (model 2).

result comes from an undetermined mistake on experimentation.

5. Validation of the analytical proposal

The effect of joint flexibility in the global structural analysis of framed structures must be considered when the joints have semi rigid behavior. However, the use of analytical equations or numerical models to estimate the initial stiffness implies a certain deviation with respect to the actual stiffness of the joints. Thus, considering a joint as a purely pinned connection when the actual stiffness is higher, implies neglect the rotational restraint of the connection. Consequently, this leads to an underestimation of the load capacity of the frame and an overestimation of the deflection. On the opposite side, considering a purely rigid connection when the actual stiffness of the joint is lower, leads to overestimate the connection restraint and thus may overestimate the load capacity of the frame or the moment in the connections. Therefore, the global structural analysis of framed structures requires a good approach to the joint stiffness to get an efficient structural design.

The Eurocode provides analytical equations which allow the joints to be classified as rigid, semi-rigid or pinned. When the stiffness of a beam-column connection in non-sway framed structures is higher than 8 times the flexural stiffness of the beam, the global structural analysis can be carried out with a nominally rigid joint. According to previous studies [33], this simplification implies a drop of no more than 5% of the critical global elastic buckling load of the frame, which corresponds to a drop of 2% of the bearing capacity of the frame.

Based on this, some authors [34,35] have proposed equations to calculate the boundaries within the difference between the actual and the approximate stiffness does not imply a drop of 5% of the critical global elastic buckling load of the braced frames (2% of the load capacity of the frame). The lower boundary (LB) can be obtained through equation (20) and the upper boundary (UB) can be obtained through equation (21).

$$LB = \frac{8 \bullet S_{j,app} \bullet E \bullet I_b}{10 \bullet E \bullet I_b + S_{j,app} \bullet L_b} \tag{20}$$

$$UB = \frac{10 \bullet S_{j,app} \bullet E \bullet I_b}{8 \bullet E \bullet I_b + S_{j,app} \bullet L_b} \tag{21}$$

Where $S_{j,app}$ is the approximate joint stiffness to be validated, E is the Young's modulus, I_b is the inertia of the beam and L_b is the length of the beam.

To determine the validity of the approximations obtained through the proposed analytical equations, the upper (UB) and lower (LB) boundaries were calculated for each type of joint, considering the approximate stiffness obtained through analytical model 2 ($S_{j,app} = S_{j,M2}$). L_b was taken equal to 20 times the depth of the beam. Next, the ratios between the real (experimental or numerical) stiffness ($S_{j,real}$) and the lower and upper border (coefficients C_1 and C_2) were calculated using expressions (22) and (23), respectively. In this way, a coefficient C_1 and C_2 lower than 1 means that the prediction is within the frontier. When both conditions are met (C_1 and C_2 less than 1), the error in the stiffness prediction does not result in a drop of more than 5% of the critical elastic buckling load. The coefficients C_1 and C_2 obtained for the tested specimens and for the joints numerically simulated can be shown in Fig. 18. The points that fall into the green area meet both conditions. As can be seen in the graph, all the joints except two of them (specimens SMS9 and DMS2) meet both conditions.

$$C_1 = \frac{LB}{S_{j,real}} \tag{22}$$

$$C_2 = \frac{S_{j,real}}{UB} \tag{23}$$

6. A fast-simplified analytical proposal for the proposed joints

When estimating preliminary stiffness of joints, simplified equations are usually required. Therefore, in this work equation (24), which makes it possible a fast preliminary sizing of the stiffness of joints with welded studs, is proposed. The equation only depends on the parameters E, which is the Young's modulus, z that is the lever arm of the joint, t_0 which is the thickness of the tube and D that is a coefficient obtained by iterating until minimizing the model error.

$$S_{j,pre} = \frac{E \bullet z^2 \bullet t_0}{D} \tag{24}$$

The equation can be applied to joints made with 10-mm and 12-mm thick angle cleats. These two thicknesses were selected due to the reason that they are available in the market for any angle cleat geometry with unequal sides. The denominator D was estimated as 39 for the specimens with a 10-mm thick angle cleat and 26 for the specimens with a 12-mm thick angle cleat. With these values, an average absolute error of 13.34% was obtained.

This simplified equation is applicable to joints in which there is only one row of studs in tension and the row consists of two studs welded to the frontal face of the column as far apart from each other as possible. This means the studs are placed as near the lateral faces of the column as possible, but taking into count the distances of the holes to the edge of the angle cleat according to the minimum and maximum distances established by Eurocode 3.(1.8) [20]. In addition, the length of the angle cleat should be equal to the width of the beam and the ratios beam width-column width should be over 0.75.

For both the tested specimens and the simulated specimens, the initial stiffness was estimated through equation (24). The estimations are shown in Table 7 and Table 8. The validity of the approximations was checked to ensure that an uncertainty in the approximation of the stiffness of the joints does not imply a drop greater than 5% of the critical global buckling elastic load, which

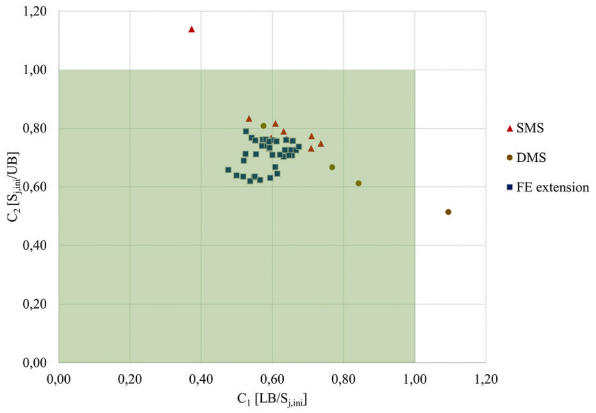

Fig. 18. Coefficients C_1 and C_2 (model 2).

Table 7
Initial stiffness obtained with the fast-simplified analytical proposal, $S_{j,pre}$, lower (LB) and upper (UB) boundaries and coefficients C_1 and C_2 calculated for the tested specimens.

Specimen	$t_l = 10$ mm		
	$S_{j,pre}$ [kNm/rad]	C_1	C_2
SMS1	1852	0.71	0.79
SMS2	2495	0.66	0.80
SMS3	3195	0.63	0.80
SMS4	3625	1.26	0.38
SMS5	4883	0.88	0.49
SMS6	6255	0.83	0.46
SMS7	3575	0.67	0.73
SMS8	4966	0.58	0.75
SMS9	6259	0.44	0.87
DMS1	2535	0.68	0.77
DMS2	3618	1.90	0.27
DMS3	4875	1.19	0.39
DMS4	4951	0.59	0.79

Table 8
Initial stiffness obtained with the fast-simplified analytical proposal, $S_{j,pre}$, lower (LB) and upper (UB) boundaries and coefficients C_1 and C_2 calculated for the numerically simulated specimens.

Joint	$t_l = 10$ mm			$t_l = 12$ mm		
	$S_{j,num}$ [kNm/rad]	C_1	C_2	$S_{j,num}$ [kNm/rad]	C_1	C_2
FEBC01	2540	0.66	0.71	3630	0.61	0.67
FEBC02	3320	0.59	0.73	5040	0.55	0.63
FEBC03	4030	0.53	0.79	6480	0.48	0.66
FEBC04	3190	0.65	0.73	4470	0.60	0.71
FEBC05	4450	0.57	0.76	6750	0.52	0.69
FEBC06	5170	0.54	0.77	8030	0.50	0.64
FEBC07	3930	0.64	0.76	5340	0.59	0.75
FEBC08	5500	0.58	0.76	8220	0.53	0.71
FEBC09	6490	0.55	0.76	9750	0.52	0.63
FEBC10	4900	0.67	0.72	6660	0.62	0.71
FEBC11	6450	0.63	0.70	9310	0.59	0.63
FEBC12	7930	0.57	0.74	11,900	0.54	0.62
FEBC13	5710	0.66	0.76	7650	0.61	0.76
FEBC14	8050	0.60	0.76	11,700	0.55	0.71
FEBC15	9350	0.59	0.74	13,900	0.55	0.63
FEBC16	7120	0.68	0.74	9430	0.64	0.73
FEBC17	9510	0.65	0.71	13,400	0.61	0.64
FEBC18	11,700	0.59	0.73	17,100	0.57	0.62

corresponds to a 2% drop in the load capacity of the frame. For this, the coefficients C_1 and C_2 were calculated again using expressions (22) and (23). The results are shown in Table 7 for the tested specimens and in Table 8 for the numerically simulated joints. All these data can be graphically seen in Fig. 19.

As it can be seen from the results, all the specimens except for three (SMS4, DMS2 and DMS3) are within the borders, which can be considered good for an initial pre-sizing stage and even acceptable for the final calculation, despite the great simplicity of the expression.

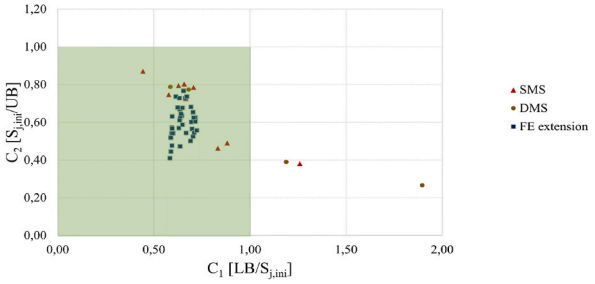

Fig. 19. Coefficients C_1 and C_2 (fast-simplified analytical proposal).

7. Conclusions

The experimental tests and the numerical simulations of the proposed flange cleated beam-RHS column joints with welded studs showed that the initial rotational stiffness of these joints increases by increasing the thickness of the tube, by increasing the parameter β (ratio between the beam width and the column width) and by increasing the depth of the beam connected to the column. All the beam-column joints were classified as semi-rigid in non-sway frames.

The tests of the beam-column joints were successfully simulated by using a simplified finite element parametric model. The elements used were Shell181 centered on the faces of the tube and on the flanges and web of the beams, while the studs were modelled by using line elements. The actual mechanical properties from some material characterization tests were used in bilinear material models. This simplifies the parametric model and decreases the computing time of the parametric extension.

The component-based analytical models proposed for the estimation of the initial stiffness of the beam-column joints present acceptable agreement with the experimental and numerical results. In addition, they both can be easily implemented in the extension of the component method to hollow section joints. Some efforts are being carried out in this sense in the most popular codes for design of joints. Comparing the analytical results with the experimental results, a higher mean absolute error was obtained for model 1 than for model 2. This means that when using specific equations for key components of the tube (model 2), the analytical stiffnesses were safer and closer to those obtained experimentally.

A simplified analytical equation to estimate the initial stiffness of the studied joints has been also proposed. This approach is useful in the pre-design of joints with threaded welded studs and very easy to apply, showing good performance with enough approximation to the results derived from experimental tests or from the extended data base from the validated numerical model.

Author statement

Ismael García: Conceptualization, Methodology, Formal analysis, Investigation, Writing - Original Draft **Miguel A. Serrano**: Conceptualization, Resources, Writing - Review & Editing, Project administration, Funding acquisition **Carlos López-Colina**: Conceptualization, Methodology, Formal analysis, validation, Writing - Review & Editing **Fernando L. Gayarre:** Resources.

Declaration of competing interest

The authors declare that they have no known competing financial interests or personal relationships that could have appeared to influence the work reported in this paper.

Data availability

Data will be made available on request.

Acknowledgements

The authors would like to acknowledge the financial support provided by the Spanish Ministry of Economy and Competitiveness through project BIA2017-83467-P, pre-doctoral grant PRE2018-084273 and by CIDECT through project 5CF. They would also like to thank the IEMES Research Group from the University of Oviedo for their support.

References

[1] J. Wardenier, J. Packer, X.-L. Zhao, G. van der Vagte, Hollow Sections in Structural Applications, 199, Technology, 2001. January 2010.
[2] L.H. Lu, J. Wardenier, Ultimate deformation criteria for uniplanar connections between I-beam and RHS columns under in-plane bending, in: Proceedings of the International Offshore and Polar Engineering Conference, 1994.
[3] L.H. Lu, The static strength of I-beam to rectangular hollow section column connections, in: Cidect Project 5AX-6/98, 1998.
[4] C. López-Colina, M.A. Serrano, M. Lozano, F.L. Gayarre, J.M. Suárez, T. Wilkinson, Characterization of the main component of equal width welded I-Beam-to-RHS-Column connections, Steel Compos. Struct. (2019), https://doi.org/10.12989/scs.2019.32.3.337.
[5] P. Rode, R. Burdett, J.C. Soares Gonçalves, Buildings: investing in energy and resource efficiency, Sustain. Dev. 19 (2011) 49–59, https://doi.org/10.1002/sd.
[6] J.K.W. Wong, J. Zhou, Enhancing environmental sustainability over building life cycles through green BIM: a Review, Autom. ConStruct. 57 (2015) 156–165, https://doi.org/10.1016/j.autcon.2015.06.003.
[7] C. Málaga-Chuquitaype, A.Y. Elghazouli, Component-based mechanical models for blind-bolted angle connections, Eng. Struct. (2010), https://doi.org/10.1016/j.engstruct.2010.05.024.
[8] A.Y. Elghazouli, C. Málaga-Chuquitaype, J.M. Castro, A.H. Orton, Experimental monotonic and cyclic behaviour of blind-bolted angle connections, Eng. Struct. (2009), https://doi.org/10.1016/j.engstruct.2009.05.021.
[9] C. Málaga-Chuquitaype, A.Y. Elghazouli, Behaviour of combined channel/angle connections to tubular columns under monotonic and cyclic loading, Eng. Struct. (2010), https://doi.org/10.1016/j.engstruct.2010.02.008.
[10] Y. Liu, C. Málaga-Chuquitaype, A.Y. Elghazouli, Response and component characterisation of semi-rigid connections to tubular columns under axial loads, Eng. Struct. 41 (2012) 510–532, https://doi.org/10.1016/j.engstruct.2012.03.061.
[11] Y. Liu, C. Málaga-Chuquitaype, A.Y. Elghazouli, Behaviour of beam-to-tubular column angle connections under shear loads, Eng. Struct. 42 (2012) 434–456, https://doi.org/10.1016/J.ENGSTRUCT.2012.04.027.
[12] R. Maquoi, X. Naveau, Beam-Column Welded Stud Connections Cidect Project 5AG, 83/5, 1983.
[13] R. Maquoi, X. Naveau, J. Rondal, Beam-column welded stud connections, J. Constr. Steel Res. (1984), https://doi.org/10.1016/0143-974X(84)90032-4.
[14] D. Vandegans, Liaison Entes Poutres Métalliques et Colonnes En Profils Creux Remplis de Béton, Basée Sur La Technique Du Goujonnage (Goujons Filetés). MT193. CRIF, 1995.
[15] D. Vandegans, Use of threaded studs in joints between I-beam and RHS-column, in: Istanbul Colloquium on Semi-rigid Connections; IABSE, Zürich, Switzerland, 1996, pp. 53–62.

[16] D. Vandegans, J. Janss, Connection between steel beams and concrete filled R.H.S. Based on the stud technique (threaded stud), *Connect. Steel Struct. III* (1996) 67–76, https://doi.org/10.1016/B978-008042821-5/50066-3.
[17] L.C. Neves, L. Simões da Silva, P.C.G. Vellasco, S. da, Experimental behaviour of end plate I-beam to concrete-filled rectangular hollow section column joints, Adv. Steel Struct. (2002) 253–260, https://doi.org/10.1016/B978-008044017-0/50029-9.
[18] M.A. Serrano-López, C. López-Colina, Y.C. Wang, M. Lozano, I. García, F.L. Gayarre, An experimental study of I beam-RHS column demountable joints with welded studs, J. Constr. Steel Res. 182 (2021), 106651, https://doi.org/10.1016/j.jcsr.2021.106651.
[19] M.A. Serrano, C. López-Colina, Y.C. Wang, M. Lozano, F. López-Gayarre, I beam-RHS column joints with welded studs, in: 9th International Conference on Steel and Aluminium Structures (ICSAS19), Independent Publishing Network, Bradford, 2019, pp. 849–860.
[20] EN 1993-1-8, Design of steel structures - Part 1-8: design of joints, Eurocode 3 (2005).
[21] W. Ramberg, W.R. Osgood, Description of stress-strain curves by three parameters, Technical Note No. 902, National Advisory Committee for Aeronautics, 1943.
[22] E. Mirambell, E. Real, On the calculation of deflections in structural stainless steel beams: an experimental and numerical investigation, J. Constr. Steel Res. 54 (1) (Apr. 2000) 109–133, https://doi.org/10.1016/S0143-974X(99)00051-6.
[24] European Committee for Standardization (CEN), EN 1993-1-5. Eurocode 3: Design of Steel Structures. Part 1-5: Plated Structural Elements, 2006.
[23] A.S.J. Foster, L. Gardner, Y. Wang, Practical strain-hardening material properties for use in deformation-based structural steel design, Thin-Walled Struct. 92 (Jul. 2015) 115–129, https://doi.org/10.1016/J.TWS.2015.02.002.
[25] M.A. Serrano-López, C. López-Colina, J. González, F. López-Gayarre, A simplified FE simulation of welded I beam-to-RHS column joints, Int. J. Steel Struct. 16 (4) (2016) 1095–1105, https://doi.org/10.1007/s13296-016-0028-5.
[26] H.T. Thai, B. Uy, Rotational stiffness and moment resistance of bolted endplate joints with hollow or CFST columns, J. Constr. Steel Res. 126 (2016) 139–152, https://doi.org/10.1016/J.JCSR.2016.07.005.
[27] G.J. Van der Vegte, J. Wardenier, R.S. Puthli, FE analysis for welded hollow-section joints and bolted joints, Proc. Inst. Civ. Eng. Struct. Build. 163 (6) (2015) 427–437, https://doi.org/10.1680/STBU.2010.163.6.427.
[28] Ungermann, D.; Schneider, S.; Trillmich, R. Tension Tests on Welded Threaded Studs with a Tensile Strength of 800N/Mm^2.
[29] D. Grotmann, G. Sedlacek, Rotational stiffness of welded RHS beam-to-column joints, in: Institute of Steel Construction, 1998. Final Report No. 5BB–8/98.
[30] C. Faella, V. Piluso, G. Rizzano, Structural Steel Semirigid Connections: Theory, Design, and Software, CRC Press, 2000.
[31] J.M. Aribert, A. Lachal, M. Moheissen, Modelling and Experimental Investigation of Plastic Resistance and Local Buckling of H or I Steel Sections Submitted to Concentrated or Partially Distributed Loading, Springer, Berlin, 1992, https://doi.org/10.1007/978-3-662-02822-3_13.
[32] M. Lozano, El Método de Los componentes Aplicado a Uniones Viga-Pilar Soldadas Entre Perfiles Abiertos y Tubo Estructural, PhD Thesis, 2019.
[33] F.S.K. Bijlaard, C. M. Steenhuis Bjorhovde, et al., Prediction of the Influence of Connection Behaviour on the Strength, Deformations and Stability of Frames, by Classification of Connections; Connections in Steel Structures II, American Institute of Steel Construction, Chigaco, 1992.
[34] J.P. Jaspart, K. Weynand, Design of Joints in Steel and Composite Structures, 2016, https://doi.org/10.1002/9783433604762.
[35] M. Steenhuis, N. Gresnigt, K. Weynand, *Pre-design of Semi-rigid Joints in Steel Frames* in Proceedings of the Second State of the Art Workshop on Semi-rigid Behaviour of Civil Engineering Structural Connections, 1994, pp. 131–140.